International Journal of Heat and Mass Transfer 99 (2016) 691–701

Contents lists available at ScienceDirect

International Journal of Heat and Mass Transfer

journal homepage: www.elsevier.com/locate/ijhmt

Effects of finite-rate droplet evaporation on the extinction of spherical burner-stabilized diffusion flames

Wang Han [a], Zheng Chen [a,b,*]

[a] SKLTCS, Department of Mechanics and Engineering Science, College of Engineering, Peking University, Beijing 100871, China
[b] Department of Aeronautics and Astronautics, College of Engineering, Peking University, Beijing 100871, China

ARTICLE INFO

Article history:
Received 6 January 2016
Received in revised form 31 March 2016
Accepted 1 April 2016

Keywords:
Droplet evaporation
Radiation
Lewis number
Spray diffusion flame
Extinction

ABSTRACT

Multiscale asymptotic analysis is conducted for spherical burner-stabilized spray diffusion flames with finite-rate droplet evaporation and nonunity Lewis number. The radiative heat loss is considered and the effects of radiation on flame extinction are examined. The structure function of the spray diffusion flame is derived, based on which the effects of finite-rate droplet evaporation on flame radius, flame temperature, and kinetic and radiative extinction limits are assessed. The flame is found to be affected by droplet evaporation in two ways: (1) the latent heat absorbed for droplet evaporation reduces the flame temperature; and (2) the decrease in the flame radius results in the decrease in radiative loss and residence time. For a given the mass flow rate, only the conventional kinetic extinction limit at low reaction Damköhler number exists. The extinction Damköhler number increases with the radiation intensity and it is significantly affected by droplet evaporation. It is found that at higher radiation intensity, the spray flame with the lower vaporization Damköhler number is relatively more difficult to be extinguished than the purely gaseous flame. When the reaction intensity is fixed and the mass flow rate varies, there exists two extinction limits: a kinetic extinction limit at a low-flow rate and a radiative extinction limit at a high-flow rate. Steady burning only exists between these two extinction limits. The flammable zone is shown to be greatly affected by droplet evaporation and is very sensitive to Lewis number.

1. Introduction

Spray diffusion flames widely exist in propulsion, heating, and power generation systems. Incomplete combustion due to extinction needs to be prevented in order to achieve high efficiency and low emission. Therefore, a fundamental understanding of the extinction mechanism in the spray diffusion flames is helpful for developing high-performance combustion systems. The practical spray combustion process contains poly-disperse sprays in turbulent flows and thereby it requires massive computational resources to simulate and capture the extinction of spray diffusion flames. However, numerical simulations are usually limited to specific fuels and conditions, and hence the conclusions are lack of generality. To get a general understanding of spray combustion, here we conduct theoretical analysis on a deliberately simplified model of spherical burner-stabilized spray diffusion flame and investigate its extinction behavior.

It is well known that flame extinction occurs when there is no enough chemical heat release to balance heat loss. For diffusion flames, there are two types of extinction: kinetic extinction and radiative extinction [1]. In the literature, the kinetic extinction of gaseous diffusion flames was extensively studied. Liñán [2] first analyzed the structure and extinction of counterflow diffusion flames with unity Lewis number and found that flame extinction occurs at a minimum reaction Damköhler number (*Da*, which is the ratio between characteristic flow time and reaction time), which is referred to as the kinetic extinction limit. The kinetic extinction was also observed in droplet combustion [3] and stagnation flame [4]. Chung and Law [5,6] generalized previous studies to different one-dimensional diffusion flames and examined the influence of nonunity Lewis number. They found that the structure function for all one-dimensional diffusion flames can be converted to the same form as that of Liñán [2] and that Liñán's extinction criteria are applicable for different diffusion flames.

Compared to kinetic extinction, radiative extinction of gaseous diffusion flames only occurs in the presence of radiative heat loss and long residence time (large *Da*). Sohrab et al. [7] first theoretically analyzed a counterflow diffusion flame with radiation by

* Corresponding author at: Department of Aeronautics and Astronautics, College of Engineering, Peking University, Beijing 100871, China.
E-mail address: cz@pku.edu.cn (Z. Chen).

http://dx.doi.org/10.1016/j.ijheatmasstransfer.2016.04.003
0017-9310/

using activation-energy-asymptotic (AEA) analysis. However, the existence of radiative extinction limit at high Damköhler number was not observed in [7] because the results are not properly rescaled. Radiative extinction limit of gaseous diffusion flame was first identified in simulation by T'ien [8], in theoretical analysis by Chao et al. [9], and in microgravity experiments by Maruta et al. [10], after which many studies were performed (e.g., [11–14]). For a spherical burned-stabilized diffusion flame considered here, its kinetic and radiative extinctions were first studied theoretically by Mills and Matalon [15,16] and then it was investigated experimentally by Yoo et al. [17], numerically and experimentally by Tse et al. [18], and numerically by Tang et al. [19,20]. More recently, Wang and Chao [21] have analyzed the kinetic and radiative extinctions of spherical burner-stabilized gaseous diffusion flames with unity Lewis number using multiscale asymptotic analysis and optically-thin radiation model for radiative heat loss. They found that strong radiation and weak reaction can greatly narrow the flammable region.

Unlike purely gaseous diffusion flames, however, spray diffusion flames receive little attention; and in the literature there are only a few studies on the extinction of spray diffusion flames. Li et al. [22] investigated the structure and extinction of counterflow spray diffusion flames with unity Lewis number. They found that the extinction state of spray diffusion flame is similar to that of purely gaseous diffusion flame. This might be caused by the assumption of unity Lewis number since small deviation of Lewis number from unity can result in significant change in the flame temperature [6,12,23]. Wichman and Yang [24] analyzed a double spray counterflow diffusion flame, in which the unity Lewis number assumption was still retained. Greenberg and coworkers [25–31] systematically examined the effects of droplet evaporation and nonunity Lewis number on the kinetic extinction of counterflow spray diffusion flames. They found that the presence of spray promotes kinetic extinction. However, in these studies [25–31], radiative heat loss was not considered and thereby the radiative extinction limit of spray diffusion flames was not observed. Santoro et al. [32,33] experimentally and numerically investigated the vortex-induced extinction behavior in the counterflow spray diffusion flames. Mikami et al. [34,35] experimentally assessed the effects of mean droplet diameter of poly-disperse water spray on the extinction of a counterflow diffusion flame. Kee and coworkers [36–39] numerically examined the flame-droplet interactions in counterflow diffusion flames. However, in these studies the radiative extinction limit was not investigated either.

To the authors' knowledge, in the literature there is no theoretical analysis on the effects of initial droplet load, finite-rate evaporation, and Lewis number on the kinetic and radiative extinction limits of spherical burner-stabilized spray diffusion flames. Therefore, the objective of this work is to examine the influence of finite-rate droplet evaporation on the kinetic and radiative extinctions of spherical spray diffusion flames with nonunity Lewis number. The emphasis is placed on examining how the flame radius, flame temperature, kinetic and radiative extinction limits, and flammable region are affected by the monodisperse droplet vaporization parameters (initial droplet load and vaporization Damköhler number), Lewis number, and radiative loss intensity.

The paper is organized as follows: the mathematical model and analytical solutions are presented in the following two sections; the behavior of spherical spray diffusion flames are investigated in Section 4; and finally, the conclusions are summarized in Section 5.

2. Mathematical model

We consider a spray diffusion flame which is stabilized by a spherical porous burner. The burner and flame structure are depicted in Fig. 1. The spherical burner-stabilized diffusion flame has been popularly adopted to study the extinction and soot formation in diffusion flames (e.g., [17–20,40–42]). Similar to that of Liu et al. [42] and Wang and Chao [21], the burner consists of a void core region ($0 < \tilde{r} < \tilde{r}_i$) in which a stream of fuel flow (containing sufficiently small fuel droplet and fuel vapor at the temperature of $\tilde{T}_0$) is supplied and a porous region ($\tilde{r}_i < \tilde{r} < \tilde{r}_b$) in which the fuel flow is regulated to be uniform at its exist. The fuel flow is steadily injected into a quiescent oxidizer environment ($\tilde{r}_b < \tilde{r} < \infty$) at the temperature of $\tilde{T}_\infty$. It is assumed that droplet evaporation is negligible until droplets leave the burner surface.

It should be emphasized that the droplets are viewed from a far-field vantage point (i.e., in the dilute spray region and accounting for a small volume fraction) in the present analysis. The interactions among the droplets are negligible and dynamic adjustment to equilibrium with their surroundings is instantaneous. Liquid phase velocity is close to that of their host velocity which refers to gas phase velocity. This simplification was validated and popularly used in previous studies [43–46]. Furthermore, the transport properties are supposed to be determined primarily by the properties of the gaseous species [43,45,46]. This follows from the implicit assumption that the liquid fuel volume fraction φ is sufficiently small, i.e., $\varphi \ll 1$. In general, the volume fraction can be of order $\varphi \sim \tilde{\rho}_g/\tilde{\rho}_l$ (in which $\tilde{\rho}_g$ and $\tilde{\rho}_l$ are density of gas phase and liquid phase, respectively) [47]. The ratio of gas density to liquid density $\tilde{\rho}_g/\tilde{\rho}_l$ found in combustion chamber is a small quantity: $10^{-3} \leqslant \varphi = \tilde{\rho}_g/\tilde{\rho}_l \leqslant 10^{-2}$ [47]. Therefore, the sufficient small volume fraction falls into the range of $10^{-3} \leqslant \varphi \leqslant 10^{-2}$. It is noted that for the porous spherical burner, there exists a long tube by which the dilute spray and gas fuel is supplied at a steady rate to the core region and hence the liquid volume fraction is also sufficiently small in the core region. For practical purposes, an upper limit on the diameter of droplets in the spray of about 50–100 μm is imposed [45] such that droplets can successfully traverse through the porous burner and then start to vaporize. Droplet burning after passing through the diffusion flame is shown to be negligible due to the small mass fraction of liquid in the initial fuel feed and thereby it is not considered in the present model. Moreover, we consider the spray diffusion flame in a microgravity environment and thereby the flame and flow field are spherically symmetrical. It is noted that the above assumptions limit the validity of results to only qualitative predictions.

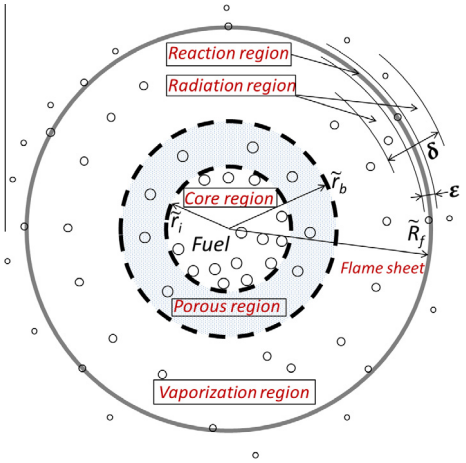

Fig. 1. The schematic diagram of spherical burner-stabilized spray diffusion flame with finite-rate vaporization of droplets (adapted from the figure for purely gaseous diffusion flame in Ref. [21]).

According to Sunderland et al. [40], the energy transfer to and from the burner due to radiation is negligible when the flame is not very close to the burner surface. Here we focus on the kinetic and radiative extinctions of spherical spray diffusion flames, which are far away from the burner surface. Therefore, radiation absorption and emission on the burner surface are not considered. Furthermore, we assume that the solid, liquid and gas phases are in thermal equilibrium inside the burner. This is a limitation of theoretical analysis compared to detailed simulation which can include the heat transfer between droplet and gas phase. Under the aforementioned assumptions, mass conservation yields a mass flow rate of $\widetilde{m} = 4\pi\widetilde{r}^2\widetilde{\rho}\widetilde{u}$ in the core region and the evaporation region, and $\widetilde{m} = 4\pi\widetilde{r}^2\widetilde{\rho}\widetilde{u}\phi$ in the porous region, where $\widetilde{m}$ is the mass flow rate; $\widetilde{\rho}$ is the mixture density defined as $\widetilde{\rho} = \widetilde{\rho}_g(1-\varphi) + \varphi\widetilde{\rho}_l$; $\widetilde{u}$ is the radial flow velocity; and ϕ is the porosity of the burner defined as the fraction of the void space in the porous media. Similar to other studies of diffusion flame stabilized by a porous burner [15,16,21,42], penetration of the ambient reactant into the burner is negligible so that reactant concentration remains unchanged inside the burner. The governing equations at different zones are

Temperature:

$$\widetilde{\rho}\widetilde{u}\widetilde{C}_p\frac{d\widetilde{T}}{d\widetilde{r}} - \frac{1}{\widetilde{r}^2}\frac{d}{d\widetilde{r}}\left(\widetilde{r}^2\widetilde{\lambda}\frac{d\widetilde{T}}{d\widetilde{r}}\right) = 0 \quad for\ 0 < \widetilde{r} < \widetilde{r}_i \tag{1}$$

$$\widetilde{\rho}\widetilde{u}\widetilde{C}_p\frac{d\widetilde{T}}{d\widetilde{r}} - \frac{1}{r^2}\frac{d}{d\widetilde{r}}\left(\widetilde{r}^2\widetilde{\lambda}_p\frac{d\widetilde{T}}{dr}\right) = 0 \quad for\ \widetilde{r}_i < \widetilde{r} < \widetilde{r}_b \tag{2}$$

$$\widetilde{\rho}\widetilde{u}\widetilde{C}_p\frac{d\widetilde{T}}{d\widetilde{r}} - \frac{1}{\widetilde{r}^2}\frac{d}{d\widetilde{r}}\left(\widetilde{r}^2\widetilde{\lambda}\frac{d\widetilde{T}}{d\widetilde{r}}\right) = \widetilde{\nu}_F\widetilde{W}_F\widetilde{q}_c\widetilde{\omega}_c - \widetilde{\omega}_r - \widetilde{q}_v\widetilde{\omega}_v \quad for\ \widetilde{r}_b < \widetilde{r} < \infty \tag{3}$$

Oxidizer:

$$\widetilde{Y}_O = 0 \quad for\ 0 < \widetilde{r} < \widetilde{r}_b \tag{4}$$

$$\widetilde{\rho}\widetilde{u}\frac{d\widetilde{Y}_O}{d\widetilde{r}} - \frac{1}{\widetilde{r}^2}\frac{d}{d\widetilde{r}}\left(\widetilde{r}^2\widetilde{\rho}\widetilde{D}_O\frac{d\widetilde{Y}_O}{d\widetilde{r}}\right) = -\widetilde{\nu}_O\widetilde{W}_O\widetilde{\omega}_c \quad for\ \widetilde{r}_b < \widetilde{r} < \infty \tag{5}$$

Gaseous fuel:

$$\widetilde{Y}_F = \widetilde{Y}_{F,0} \quad for\ 0 < \widetilde{r} < \widetilde{r}_b \tag{6}$$

$$\widetilde{\rho}\widetilde{u}\frac{d\widetilde{Y}_F}{d\widetilde{r}} - \frac{1}{\widetilde{r}^2}\frac{d}{d\widetilde{r}}\left(\widetilde{r}^2\widetilde{\rho}\widetilde{D}_F\frac{d\widetilde{Y}_F}{d\widetilde{r}}\right) = -\widetilde{\nu}_F\widetilde{W}_F\widetilde{\omega}_c + \widetilde{\omega}_v \quad for\ \widetilde{r}_b < \widetilde{r} < \infty \tag{7}$$

Liquid fuel:

$$\widetilde{Y}_d = \widetilde{Y}_{d,0} \qquad for\ 0 < \widetilde{r} < \widetilde{r}_b \tag{8}$$

$$\widetilde{\rho}\widetilde{u}\frac{d\widetilde{Y}_d}{d\widetilde{r}} = -\widetilde{\omega}_v \quad for\ \widetilde{r}_b < \widetilde{r} < \infty \tag{9}$$

where $\widetilde{T}, \widetilde{Y}_O, \widetilde{Y}_F$, and $\widetilde{Y}_d$ are temperature of mixture, mass fraction of oxidizer, mass fraction of gaseous fuel, and mass fraction of liquid fuel, respectively; $\widetilde{r}$ is spatial coordinate; $\widetilde{r}_i$ and $\widetilde{r}_b$ are respectively the inner and outer radii of the burner as shown in Fig. 1; $\widetilde{\nu}_F$ and $\widetilde{\nu}_O$ are stoichiometric coefficients of fuel and oxidizer, respectively; $\widetilde{W}_F$ and $\widetilde{W}_O$ are the molecular weight of fuel and oxidizer, respectively; $\widetilde{Y}_{F,0}$ and $\widetilde{Y}_{d,0}$ are the mass fractions of gas fuel and droplet fuel in the center of burner, respectively. The parameters, $\widetilde{q}_c$ and $\widetilde{q}_v$, denote the reaction heat-release per unit mass of fuel and the latent heat of evaporation, respectively. The heat capacity $\widetilde{C}_p$, heat conductivity $\widetilde{\lambda}$ of the gas–liquid mixture, heat conductivity of the solid burner $\widetilde{\lambda}_p$, molecular diffusivity $\widetilde{D}_F$ of the gaseous fuel and molecular diffusivity $\widetilde{D}_O$ of oxidizer are all assumed to be constant. According to the thermal equilibrium assumption, the equivalent heat conductivity in the porous burner is $\widetilde{\lambda}_p = \widetilde{\lambda}\phi + \widetilde{\lambda}_p(1-\phi)$.

A global one-step irreversible reaction described by the Arrhenius law is employed. The reaction is assumed to be first order with respect to both fuel and oxidizer. Its reaction rate is

$$\widetilde{\omega}_c = \widetilde{\rho}^2\widetilde{A}\widetilde{Y}_F\widetilde{Y}_O\exp(-\widetilde{T}_c/\widetilde{T}) \tag{10}$$

where $\widetilde{A}$ is the pre-exponential factor and $\widetilde{T}_c$ the activation temperature for reaction.

In the limit of large but finite activation energy, the reaction rate is very sensitive to temperature and chemical reaction occurs only in a thin reaction region where the temperature is close to the maximum temperature or flame temperature, $\widetilde{T}_f$ [1]. Away from the reaction region, chemical reaction is frozen. Similar to chemical reaction, radiative loss from the flame is also sensitive to temperature ($\sim \widetilde{T}^4$) and thereby it is significant only in a thin radiation region near the reaction region. Therefore, radiative loss can be approximated by an Arrhenius function [7,21,48] in the following form:

$$\widetilde{\omega}_r = \widetilde{A}_r\exp(-\widetilde{T}_r/\widetilde{T}) \tag{11}$$

where $\widetilde{A}_r$ is the equivalent pre-exponential factor and $\widetilde{T}_r$ the equivalent activation temperature for radiative loss. Because the equivalent activation temperature of the radiative loss is much lower than that of chemical reaction (i.e., $\widetilde{T}_r \ll \widetilde{T}_c$), the thickness of radiation region (in which radiation is significant) is much larger than the thickness of reaction region. Based on the above discussion on length scales, the region outside of the burner is further divided into five sub-regions. As depicted in Fig. 1, the thin reaction region embedding the flame sheet is sandwiched by two radiation regions, which are surrounded by two broad vaporization regions. It is noted that droplet vaporization is not important in the radiation and reaction regions since the amount of vaporization is proportion to the volume. Similarly, radiation is neglected in the thin reaction region. The characteristic length of the reaction region (normalized by the length of the vaporization region) is ϵ and that of the radiation region is δ. Therefore, we have $\epsilon \ll \delta \ll 1$ since $\widetilde{T}_c \gg \widetilde{T}_r \gg 1$. The small parameters ϵ and δ are used in the following multiscale asymptotic expansions.

We adopt the sectional approach to model poly-disperse spray [49–52]. The details on sectional approach can be found in [49–51]. In order to simply assess the effects of primary spray parameters (vaporization rate and initial droplet load), the concept of a quasi-mono-disperse spray [45,46,52] (i.e., containing droplets of approximately the same size) is used here. Under the above simiplification, the finite evaporation rate, $\widetilde{\omega}_v$ in Eqs. (3), (7) and (9) is

$$\widetilde{\omega}_v = \widetilde{\rho}\widetilde{C}\widetilde{Y}_d \tag{12}$$

where $\widetilde{Y}_d$ is the mass fraction of droplets and $\widetilde{C}$ is the sectional vaporization coefficient [50,46]. It is noted that the quasi-monodisperse spray model has an apparent disadvantage due to artificially designating all the droplets in a single size and neglecting the details of the spray's actual size distribution. Nevertheless, the usage of the quasi-monodisperse spray model is indeed capable of providing essential elements of the processes of heat and mass transfer from the spray to its host gas so that, at least, qualitative conclusions can be drawn [45,46,52].

The following variables are introduced to normalize Eqs. (1)–(9):

$$r = \frac{\widetilde{r}}{\widetilde{r}_b}, \quad T = \frac{\widetilde{C}_p\widetilde{T}}{\widetilde{q}_c(\widetilde{Y}_{F,0} + \widetilde{Y}_{d,0})}, \quad Y_F = \frac{\widetilde{Y}_F}{\widetilde{Y}_{F,0} + \widetilde{Y}_{d,0}} \tag{13}$$

$$Y_O = \frac{\widetilde{\nu}_F\widetilde{W}_F\widetilde{Y}_O}{\widetilde{\nu}_O\widetilde{W}_O(\widetilde{Y}_{F,0} + \widetilde{Y}_{d,0})}, \quad m = \frac{\widetilde{C}_p\widetilde{m}}{4\pi\widetilde{r}_b\widetilde{\lambda}}, \quad \lambda_p = \phi + (1-\phi)\frac{\widetilde{\lambda}_p}{\widetilde{\lambda}} \tag{14}$$

which yields the non-dimensional governing equations as follows:

Temperature:

$$\frac{1}{r^2}\frac{d}{dr}\left(mT - r^2\frac{dT}{dr}\right) = 0 \quad for\ 0 < r < r_i \tag{15}$$

$$\frac{1}{r^2}\frac{d}{dr}\left(mT - \lambda_p r^2\frac{dT}{dr}\right) = 0 \quad for\ r_i < r < 1 \tag{16}$$

$$\frac{1}{r^2}\frac{d}{dr}\left(mT - r^2\frac{dT}{dr}\right) = \omega_c - \omega_r - q_v\omega_v \quad for\ 1 < r < \infty \tag{17}$$

Oxidizer:

$$Y_O = 0 \quad for\ 0 < r < 1 \tag{18}$$

$$\frac{1}{r^2}\frac{d}{dr}\left(mY_O - \frac{1}{Le_O}r^2\frac{dY_O}{dr}\right) = -\omega_c \quad for\ 1 < r < \infty \tag{19}$$

Gaseous fuel:

$$Y_F = 1 - \Delta \quad for\ 0 < r < 1 \tag{20}$$

$$\frac{1}{r^2}\frac{d}{dr}\left(mY_F - \frac{1}{Le_F}r^2\frac{dY_F}{dr}\right) = -\omega_c + \omega_v \quad for\ 1 < r < \infty \tag{21}$$

Liquid fuel:

$$Y_d = \Delta \quad for\ 0 < r < 1 \tag{22}$$

$$\frac{1}{r^2}\frac{d}{dr}(mY_d) = -\omega_v \quad for\ 1 < r < \infty \tag{23}$$

where $Le_F = \widetilde{\lambda}/(\widetilde{\rho}\widetilde{C}_p\widetilde{D}_F)$ and $Le_O = \widetilde{\lambda}/(\widetilde{\rho}\widetilde{C}_p\widetilde{D}_O)$ are respectively the Lewis numbers of fuel and oxidizer. Δ is the initial droplet load defined as $\Delta = \widetilde{Y}_{d,0}/(\widetilde{Y}_{F,0} + \widetilde{Y}_{d,0})$. q_v represents the normalized latent heat of evaporation, which is defined as $q_v = \widetilde{q}_v/\widetilde{q}_c$. The non-dimensional source terms take the following forms

$$\omega_c = Da_K Y_F Y_O \exp(-T_c/T), \quad \omega_r = Da_R \exp(-T_r/T), \quad \omega_v = Da_V Y_d \tag{24}$$

where $Da_K = \widetilde{\nu}_O\widetilde{W}_O\widetilde{A}\widetilde{\rho}^2\widetilde{C}_p\widetilde{r}_b^2(\widetilde{Y}_{F,0} + \widetilde{Y}_{d,0})/\widetilde{\lambda}$ is the reaction Damköhler number; $Da_R = \widetilde{A}_r\widetilde{C}_p\widetilde{r}_b^2/[\widetilde{q}_c\widetilde{\lambda}(\widetilde{Y}_{F,0} + \widetilde{Y}_{d,0})]$ the equivalent radiation Damköhler number; and $Da_V = \widetilde{\rho}\widetilde{C}\widetilde{C}_p\widetilde{r}_b^2/\widetilde{\lambda}$ the vaporization Damköhler number which is proportional to the volatility of the fuel and inversely proportional to the size of the droplets in the spray. Thus, the extent of droplet evaporation depends on Da_V. The flow time scale, $\tau_{flow} = \widetilde{\rho}\widetilde{C}_p\widetilde{r}_b^2/\widetilde{\lambda}$, is used in the above definitions of Damköhler numbers. It is noted that the vaporization Damköhler number, Da_V, strongly depends on the temperature and the volume of the droplet and also varies in the radial direction because of the temperature gradient. In the present work, the simplification of constant vaporization Damköhler number is made to obtain the analytical solutions. It has been shown that [45,46] this simplification does not affect the qualitative nature of the predictions. For spray with high volatility and/or small droplet size, the vaporization Damköhler number is larger than 10^{-4}. Conversely, for spray with low volatility or large droplet size, the vaporization Damköhler number is in the range of $10^{-8} < Da_V < 10^{-4}$ [45,46,52].

Eqs. (15)–(23) are subject to the following boundary and interfacial conditions:

$$r = 0 : T = T_0 = T_\infty. \tag{25}$$

$$r = r_i : T = T_i, \quad \left(\frac{dT}{dr}\right)_{r_i^-} = \lambda_p\left(\frac{dT}{dr}\right)_{r_i^+}. \tag{26}$$

$$T = T_b, \quad \lambda_p\left(\tfrac{dT}{dr}\right)_{1^-} = \left(\tfrac{dT}{dr}\right)_{1^+},$$

$$r = 1 : mY_F/r^2 - Le_F^{-1}\tfrac{dY_F}{dr} = m(1-\Delta)/r^2, \tag{27}$$

$$mY_O/r^2 - Le_O^{-1}\tfrac{dY_O}{dr} = 0, \quad Y_d = \Delta.$$

$$r \to \infty : T = T_\infty, \quad Y_F \to 0, \quad Y_O \to Y_{O,\infty}, \quad Y_d \to 0. \tag{28}$$

where the temperatures at the inner and outer surfaces of the spherical burner, T_i and T_b, are to be determined in the following analysis.

3. Multiscale asymptotic analysis

3.1. Core zone and porous zone

Owing to the constant mass fraction for each species, only governing equations of temperature need to be solved in this zone. The solutions to the temperature Eqs. (15) and (16) subject to the appropriate boundary and interfacial conditions in Eqs. (25)–(27) are

$$T = \begin{cases} T_\infty + (T_i - T_\infty)\exp\left[m(r_i^{-1} - r^{-1})\right] & for\ 0 < r < r_i \\ T_i + (T_b - T_i)\frac{\exp\left[-m/(\lambda_p r)\right] - \exp\left[-m/(\lambda_p r_i)\right]}{\exp\left[-m/(\lambda_p)\right] - \exp\left[-m/(\lambda_p r_i)\right]} & for\ r_i < r < 1 \end{cases} \tag{29}$$

Substituting Eq. (29) into Eq. (26) yields the following expression for the temperature at the inner surface of the burner, T_i, in term of T_b

$$T_i = T_\infty + (T_b - T_\infty)\exp\left[(m/\lambda_p)(1 - r_i^{-1})\right]. \tag{30}$$

3.2. Vaporization zone

Since $\epsilon \ll \delta \ll 1$, the equations for temperature and species outside of the burner (i.e., $1 < r < \infty$) are solved by multiscale asymptotic analysis. The region outside of the burner is divided into three parts: outer zone (i.e., vaporization zone), radiation zone and reaction zone. In the outer zone, the conservation equations are governed by the balance between diffusion, convection and vaporization processes. The droplet mass fraction distribution in the vaporization region is

$$Y_d = \Delta\exp\left[Da_V(1 - r^3)/(3m)\right] \tag{31}$$

Expanding the solutions in term of the small expansion parameters ϵ and δ [21] as follows

$$T^\pm = \left[T_0^\pm + \epsilon T_1^\pm + O(\epsilon^2)\right] + \delta\left[T_2^\pm + O(\epsilon)\right] + O(\delta^2) \tag{32}$$

$$Y_F^\pm = \left[Y_{F,0}^\pm + \epsilon Y_{F,1}^\pm + O(\epsilon^2)\right] + \delta\left[Y_{F,2}^\pm + O(\epsilon)\right] + O(\delta^2) \tag{33}$$

$$Y_O^\pm = \left[Y_{O,0}^\pm + \epsilon Y_{O,1}^\pm + O(\epsilon^2)\right] + \delta\left[Y_{O,2}^\pm + O(\epsilon)\right] + O(\delta^2) \tag{34}$$

and combining the boundary conditions in Eqs. (27) and (28), we have the following solutions in the outer zone

$$\begin{cases} T_0^- = T_\infty + (T_{b,0} - T_\infty)\exp\left[m(1 - r^{-1})\right] + \int_1^r I_T(r,\tau)\,d\tau & (35) \\ T_i^- = T_{b,i}\exp\left[m(1 - r^{-1})\right] \ldots i = 1,2 & (36) \\ T_0^+ = T_\infty + a_{T,0}^+[(1 - \exp(-m/r)] + \int_\infty^r I_T(r,\tau)\,d\tau & (37) \\ T_i^+ = a_{T,i}^+[1 - \exp(-m/r] \ldots i = 1,2 & (38) \end{cases}$$

where $I_T(r,\tau) = q_v Da_V\frac{\exp(-m/r) - \exp(-m/\tau)}{m\exp(-m/\tau)}\tau^2 Y_d(\tau)$.

$$\begin{cases} Y_{F,0}^- = 1 - \Delta - a_{F,0}^-\exp(-mLe_F/r) + \int_1^r I_F(r,\tau)\,d\tau & (39) \\ Y_{F,i}^- = -a_{F,i}^-\exp(-mLe_F/r) \ldots i = 1,2 & (40) \\ Y_{F,0}^+ = a_{F,0}^+[1 - \exp(-mLe_F/r)] + \int_\infty^r I_F(r,\tau)\,d\tau & (41) \\ Y_{F,i}^+ = a_{F,i}^+[1 - \exp(-mLe_F/r)] \ldots i = 1,2 & (42) \end{cases}$$

where $I_F(r,\tau) = Da_V\frac{\exp(-mLe_F/\tau) - \exp(-mLe_F/r)}{m\exp(-mLe_F/\tau)}\tau^2 Y_d(\tau)$.

$$\begin{cases} Y_{O,i}^- = a_{O,i}^-\exp(-mLe_O/r) \ldots i = 0,1,2 & (43) \\ Y_{O,0}^+ = Y_{O,\infty} - a_{O,0}^+[1 - \exp(-mLe_O/r)] & (44) \\ Y_{O,i}^+ = -a_{O,i}^+[1 - \exp(-mLe_O/r)] \ldots i = 1,2 & (45) \end{cases}$$

In the above expressions, we designate the variables between the burner and flame by superscript "−" and variable outside of the flame by "+", respectively. The *a*'s are integration constants yet to be determined. The equations are not completely solved since there is only one boundary condition on each side of the reaction zone.

3.3. Radiation zone

In the $O(\delta)$ radiation zone, radiative loss is considered and the flame temperature T_f is reduced by the amount of $O(\delta)$. Chemical reaction is still negligible and thereby the outer solutions of $Y_F^{\pm}$ and $Y_O^{\pm}$ are also applicable. In the radiation zone, we introduce a stretched coordinate, $\xi = (r - R_f)/\delta$, in which δ is defined as $\delta = T_f^2/T_r$ and R_f is flame radius. The temperature is expanded as [21]

$$T^{\pm} = \left[T_f - \epsilon\Theta_2^{\pm} + O(\epsilon^2)\right] - \delta\left[\Theta_1^{\pm} + \epsilon\Theta_3^{\pm} + O(\delta^2)\right] \tag{46}$$

Substituting the above temperature expansion into the Eq. (17) yields the following governing equations of temperature in the radiation zone:

$$\begin{cases} \frac{d^2\Theta_1^{\pm}}{d\xi^2} = -\Lambda_R \exp(-\Theta_1^{\pm}) & (47)\\ \frac{d^2\Theta_2^{\pm}}{d\xi^2} = \Lambda_R\Theta_2^{\pm} \exp(-\Theta_1^{\pm}) & (48)\\ \frac{d^2\Theta_3^{\pm}}{d\xi^2} = \frac{m-2R_f}{R_f^2}\frac{d\Theta_2^{\pm}}{d\xi} + \Lambda_R\left(\Theta_3^{\pm} + \frac{2\Theta_1^{\pm}\Theta_2^{\pm}}{T_f}\right)\exp(-\Theta_1^{\pm}) & (49)\end{cases}$$

where $\Lambda_R = \delta Da_R \exp(-T_r/T_f)$ is the equivalent reduced radiation Damköhler number.

The boundary conditions for Eqs. (47)-(49) can be obtained from matching the solutions of temperature in the outer zone with those in the radiation zone as $r \to R_f$. Through the matching process, we first obtain the following solutions for two constants, $T_{b,0}$ and $a_{T,0}^+$, in term of T_f

$$T_{b,0} = T_\infty + [T_f - T_\infty - \int_1^{R_f} I_T(R_f,\tau)\,d\tau]/\exp[m(1-R_f^{-1})] \tag{50}$$

$$a_{T,0}^+ = [T_f - T_\infty - \int_\infty^{R_f} I_T(R_f,\tau)\,d\tau]/[1-\exp(-m/R_f^{-1})] \tag{51}$$

Integrating Eqs. (47) and (48) and using the matching conditions yields

$$\begin{cases} \Theta_1^{\pm} = 2\ln[1 - 0.5\Lambda_R \exp(g_1^{\pm} \mp g_0^{\pm}\xi)/(g_0^{\pm})^2] \pm g_0^{\pm}\xi - g_1^{\pm} & (52)\\ \Theta_2^{-} = (T_{b,1}/g_0^{-})\exp[(m(1-R_f^{-1})]\frac{d\Theta_1^{-}}{d\xi} & (53)\\ \Theta_2^{+} = -(a_{T,1}^{+}/g_0^{-})[1-\exp(-m/R_f)]\frac{d\Theta_1^{+}}{d\xi} & (54)\end{cases}$$

where

$$\begin{cases} g_0^{-} = [T_f - T_\infty - \int_1^{R_f} I_T\,d\tau] + \frac{q_v Da_V}{R_f^2}\int_1^{R_f}[Y_d\tau^2\exp(m/\tau - m/R_f)]\,d\tau\\ g_0^{+} = \frac{m}{R_f^2}\frac{T_f - T_\infty - \int_\infty^{R_f} I_T\,d\tau}{\exp(m/R_f)-1} - \frac{q_v Da_V}{R_f^2}\int_\infty^{R_f}[Y_d\tau^2\exp(m/\tau - m/R_f)]\,d\tau\\ g_1^{+} = T_{b,2}\exp[m(1-R_f^{-1})]\\ g_1^{+} = a_{T,2}^{+}[1-\exp(-m/R_f)]\end{cases} \tag{55}$$

3.4. Reaction zone

In the $O(\epsilon)$ reaction zone, only $O(\epsilon)$ variations of variables and an $O(\epsilon)$ leakage of reactants are allowed. As a result, the temperature is within an $O(\epsilon)$ reduction from the maximum temperature T_f and the reactant mass fraction are $O(\epsilon)$ quantities. In order to analyze the flame structure, we introduce a stretched spatial coordinate, $\zeta = (r - R_f)/\epsilon$, in which $\epsilon = T_f^2/T_c$. The temperature, fuel and oxidizer mass fractions are expanded as [21]

$$T = \left[T_f - \epsilon\theta_1 - \epsilon^2\theta_2 + O(\epsilon^3)\right] + O(\delta) + O(\epsilon/\delta) \tag{56}$$

$$Y_F = \left[\epsilon\psi_{F,1} + \epsilon^2\psi_{F,2} + O(\epsilon^3)\right] + O(\delta) + O(\epsilon/\delta) \tag{57}$$

$$Y_O = \left[\epsilon\psi_{O,1} + \epsilon^2\psi_{O,2} + O(\epsilon^3)\right] + O(\delta) + O(\epsilon/\delta) \tag{58}$$

Substituting the stretched coordinate, $\zeta = (r - R_f)/\epsilon$, and Eqs. (56)–(58) into Eqs. (15)–(21) and expanding and collecting the leading-order terms of ϵ and δ, we obtain the following flame structure equation, species-species coupling functions, and temperature-species coupling functions in the reaction zone

$$\frac{d^2\theta_1}{d\zeta^2} = \Lambda_K\psi_{F,1}\psi_{O,1}\exp(-\theta_1) \tag{59}$$

$$Le_F^{-1}\psi_{F,1} - Le_O^{-1}\psi_{O,1} = C_1\zeta + C_2 \tag{60}$$

$$\frac{d\left(Le_F^{-1}\psi_{F,2} - Le_O^{-1}\psi_{O,2}\right)}{d\zeta} + \frac{2}{R_f}\frac{d\left(Le_F^{-1}\psi_{F,1} - Le_O^{-1}\psi_{O,1}\right)}{d\zeta} - \frac{m}{R_f^2}(\psi_{F,1} - \psi_{O,1}) = C_3 \tag{61}$$

$$\theta_1 - Le_F^{-1}\psi_{F,1} = C_4\zeta + C_5 \tag{62}$$

$$\frac{d\left(\theta_2 Le_F^{-1}\psi_{F,2}\right)}{d\zeta} + \frac{2}{R_f}\frac{d(\theta_1 - Le_F^{-1}\psi_{F,1})}{d\zeta} - \frac{m}{R_f^2}(\theta_1 - Le_F^{-1}\psi_{F,1}) = C_6 \tag{63}$$

where $\Lambda_K = \epsilon^2 Da_K \exp(-T_c/T_f)$ is the reduced reaction Damköhler number and the *C*'s are integration constants to be determined.

Similar to the analysis of radiation zone, the boundary conditions for Eqs. (59)–(63) are derived from matching the inner solutions in the limits of $\zeta \to \pm\infty$ with the outer solutions of Y_F and Y_O in the limit of $r \to R_f$ and with the solutions of T in the radiation zone in the limit of $\xi \to 0$. Among them

$$\theta_1(\zeta \to -\infty) = -\left\{\frac{T_{b,1}}{g_0^{-}}\exp[m(1-R_f^{-1})] + \zeta\right\}\sqrt{(g_0^{-})^2 + 2\Lambda_R} \tag{64}$$

$$\theta_1(\zeta \to +\infty) = -\left\{\frac{a_{T,1}^{+}}{g_0^{+}}[1-\exp(-m/R_f^{-1})] - \zeta\right\}\sqrt{(g_0^{+})^2 + 2\Lambda_R} \tag{65}$$

are required to solve Eq. (59). The matching also gives

$$\begin{cases} a_{F,0}^{-} = \left[1 - \Delta + \int_1^{R_f} I_F\,d\tau\right]\exp(mLe_F/R_f)\\ a_{F,0}^{+} = -\int_1^{R_f} I_F\,d\tau/[1-\exp(-mLe_F/R_f)]\\ -a_{F,1}^{+} = a_{O,1}^{+} = \left(a_{T,1}^{+}/g_0^{+}\right)\sqrt{(g_0^{+})^2 + 2\Lambda_R}\\ a_{F,2}^{+} = a_{F,2}^{+} = a_{O,0}^{-} = a_{O,2}^{-} = a_{O,2}^{+} = 0\\ a_{O,0}^{+} = Y_{O,\infty}/\left[1-\exp(-mLe_O/R_f)\right]\end{cases} \tag{66}$$

In addition, in the matching process we obtain the following expressions for flame radius R_f and flame temperature T_f:

$$\frac{Y_{O,\infty}}{\exp(mLe_O/R_f) - 1} = 1 - \Delta + \int_1^{R_f} I_F\,d\tau + \frac{Da_V\int_1^{R_f} I_F'(\tau)\,d\tau}{m} + \frac{\int_\infty^{R_f} I_F\,d\tau}{\exp(mLe_F/R_f) - 1} \tag{67}$$

$$\frac{m}{R_f^2}\frac{Y_{O,\infty}}{\exp(mLe_O/R_f) - 1} = \sqrt{(g_0^{-})^2 + 2\Lambda_R} + \sqrt{(g_0^{+})^2 + 2\Lambda_R} \tag{68}$$

where $I_F'(\tau) = Y_d\tau^2\exp(mLe_F/\tau - mLe_F/R_f)$.

It is noted that the flame radius and flame temperature are both independent of the burner size. For purely gaseous adiabatic spherical diffusion flames, Eqs. (67) and (68) reduce to that under adiabatic condition:

$$R_f^{ad,gas} = mLe_O/\ln(1+Y_{O,\infty}) \tag{69}$$

$$T_f^{ad,gas} = T_\infty + Y_{O,\infty}/(1+Y_{O,\infty}) \tag{70}$$

The reactant leakage across the flame can be represented by

$$Y_{F,L} = Y_{F,1}^+(R_f) = a_{F,1}^+[1-\exp(-mLe_F/R_f)] \tag{71}$$

and the first order quantities of oxidizer and fuel can be expressed in the first order quantities of temperature

$$Le_O^{-1}\psi_{O,1} = \theta_1 + \sqrt{(g_0^-)^2+2\Lambda_R}\zeta - (a_{T,1}^+/g_0^+)\sqrt{(g_0^+)^2+2\Lambda_R} \times [Le_O^{-1} - 1 + e^{-m/R_f} - Le_O^{-1}e^{-mLe_O/R_f}] \tag{72}$$

$$Le_F^{-1}\psi_{F,1} = \theta_1 - \left\{\sqrt{(g_0^+)^2+2\Lambda_R} - \frac{m}{R_f^2}\int_\infty^{R_f} I_F\,d\tau/[e^{mLe_F/R_f}-1]\right\}\zeta - (a_{T,1}^+/g_0^+)\sqrt{(g_0^+)^2+2\Lambda_R}\left[Le_F^{-1} - 1 + e^{-m/R_f} - Le_F^{-1}e^{-mLe_F/R_f}\right] \tag{73}$$

For simplicity, we assume that the Lewis number of the fuel is equal to that of the oxidizer, i.e., $Le_F = Le_O = Le$. As a result, the equations containing Eqs. (59), (64),(65), and (72),(73) can be converted to Liñán's equations in diffusion flame regime [2]. Similar to [9,21], the conversion is performed by introducing a new independent variable ζ_L and a new dependent variable θ_L as

$$\zeta_L = (\alpha^{1/3}\beta/2)\zeta \tag{74}$$

$$\theta_L = \alpha^{1/3}(\theta_1 + a_{F,1}^+\ell e) - \gamma\zeta \tag{75}$$

where

$$\begin{cases} \alpha &= (2Le/\beta)^2\Lambda_K\exp(\ell e + a_{F,1}^+) \\ \beta &= (m/R_f^2)[1-\Delta+\int_1^{R_f} I_F\,d\tau] + (Da_V/R_f^2)\int_1^{R_f} I_F'\,d\tau \\ \gamma &= 1-(2/\beta)\sqrt{(g_0^+)^2+2\Lambda_R} \\ \ell &= (m/R_f^2)\int_\infty^{R_f} I_F\,d\tau/[\exp(mLe/R_f)-1] \\ \ell e &= Le^{-1} - 1 + e^{-m/R_f} - Le^{-1}e^{-mLe/R_f} \end{cases} \tag{76}$$

Substituting Eqs. (74) and (75) to Eqs. (59), (64),(65), and (72), (73) yields

$$\frac{d^2\theta_L}{d\zeta_L^2} = (\theta_L+\zeta_L)(\theta_L-\zeta_L)\exp[-\alpha^{1/3}(\theta_L+\gamma\zeta_L)] \tag{77}$$

$$\frac{d\theta_L}{d\zeta_L} = -1 \quad (\zeta_L\to-\infty) \tag{78}$$

$$\frac{d\theta_L}{d\zeta_L} = 1+2\ell/\beta \quad (\zeta_L\to+\infty) \tag{79}$$

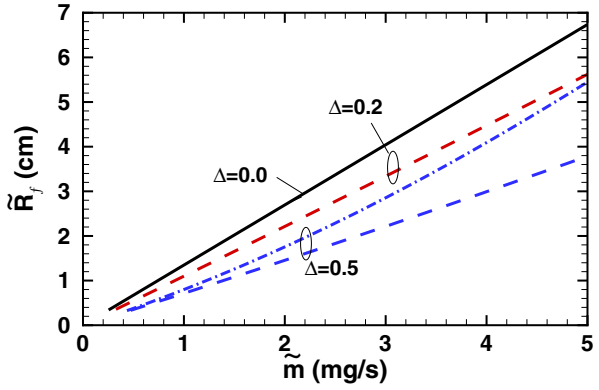

Fig. 2. Change of flame radius, $\widetilde{R}_f$, with mass flow rate, $\widetilde{m}$, at $Le = 1.0$. Dashed lines: $Da_V = 10^{-6}$; dash-dotted lines: $Da_V = 10^{-4}$.

and the constants $T_{b,1}$ and $a_{T,1}^+$ are determined by the following two expressions, respectively:

$$\theta_L(\zeta_L\to-\infty) = -\frac{\alpha^{1/3}T_{b,1}}{g_0^-}e^{m(1-R_f^{-1})}\sqrt{(g_0^-)^2+2\Lambda_R} + a_{F,1}^+\ell e - \zeta_L \tag{80}$$

$$\theta_L(\zeta_L\to+\infty) = \alpha^{1/3}Y_{F,L} + a_{F,1}^+\ell e + (1+2\ell/\beta)\zeta_L \tag{81}$$

When there is no droplet load and the Lewis numbers of fuel and oxidizer are unity (i.e. $\Delta = 0$ and $Le = 1.0$), Eqs. (77)–(81) reduces to previous results on purely gaseous spherical diffusion flame in [21]. Therefore, the present analysis is consistent with that in previous study on purely gaseous diffusion flames. By numerically solving Eqs. (77)–(81) using the fourth order Runge–Kutta method and Newton's iteration method, the kinetic and radiative extinction conditions of spherical burner-stabilized spray diffusion flames can be obtained.

4. Results and discussion

In this study, the thermal and transport parameters are chosen to n-decane/air mixture. They are $\widetilde{T}_0 = \widetilde{T}_\infty = 298$ K, $\widetilde{q}_c = 69920$ J/g, $\widetilde{C}_p = 2.2215$ J/(g·K), $\widetilde{\nu}_F = 1, \widetilde{\nu}_O = 15.5$, $\widetilde{\lambda} = 0.0012043$ W/(cm·K), $\widetilde{W}_F = 142$ g/mole, $\widetilde{W}_O = 32$ g/mole, $\widetilde{T}_c = 15089$ K, $\widetilde{T}_r = 8000$ K, $\widetilde{r}_b = 0.3175$ cm (the burner size is chosen as the one used in experiments by Sunderland et al. [40,41]).

Based on these data and Eq. (70), the purely gaseous flame temperature is $T_f^{ad,gas} = 2292$ K. In addition, the latent heat of vaporization is taken to be $q_v = 0.1q_c$, which is chosen for n-decane fuel according to Lefebvre [53]. The above data can be replaced by other values when other fuels or burner sizes are interested.

It is noted that the quantifying parameters, $\delta, \epsilon, \Lambda_R$, and Λ_K, depend on the leading-order flame temperature T_f, which changes with the radiative loss intensity and droplet load. Therefore, the same nondimensional value can correspond to different cases with different physical parameters, which make the above theoretical analysis not amenable for ready interpretation of the system behavior. According to Chao et al. [9,21], it is necessary to rescale all the parameters to a fixed, absolute reference state. The obvious choice of the reference state is the adiabatic purely gaseous state. Designating properties nondimensionalized by these reference quantities by the superscript "*", we have $T_f^* = T_\infty^* + Y_{O,\infty}^*/(1+Y_{O,\infty}^*)$, $\delta^* = T_f^{*2}/T_r^*$, $\epsilon^* = T_f^{*2}/T_c^*$, $\Lambda_R^* = \delta^* Da_R^*\exp(-T_r^*/T_f^*)$, $\Lambda_K^* = \epsilon^{*3}Da_K^*\exp(-T_c^*/T_f^*)$.

With these rescaled parameters, the parameters required to present the results can be rescaled to

$$\Lambda_R = \Lambda_R^*(T_f/T_f^*)^2\exp(T_r^*/T_f^* - T_r/T_f) \tag{82}$$

$$\Lambda_K = \Lambda_K^*(T_f/T_f^*)^6\exp(T_c^*/T_f^* - T_c/T_f) \tag{83}$$

$$Y_{F,L} = Y_{F,L}^*/(T_f/T_f^*)^2 \tag{84}$$

It is noted that in the rescaled process we have $Da_R^* = Da_R, Da_K^* = Da_K, T_r^* = T_r$, and $T_c^* = T_c$.

4.1. Flame radius and flame temperature

We first investigate the effects of radiative loss and droplet evaporation on the flame radius and flame temperature, both of which are determined by the leading order (i.e., zeroth order) solutions which are obtained by assuming the reaction rate to be infinitely fast.

Fig. 2 shows the change of flame radius, $\widetilde{R}_f$, with mass flow rate, $\widetilde{m}$, for different values of fuel droplet load and vaporization Damköhler number. These quantities are presented in their

physical values instead of non-dimensional forms. For purely gaseous flame (i.e., $\Delta = 0$), the flame radius, $\widetilde{R}_f$, is shown to change linearly with the mass flow rate, $\widetilde{m}$, as predicted by Eq. (69). The same trend was also obtained in [21]. However, for spray flame, $\widetilde{R}_f$ does not changes linearly with $\widetilde{m}$ and the presence of droplets reduces the flame radius at a given value of $\widetilde{m}$. This is because the gaseous fuel concentration is reduced when there are fuel droplets. Furthermore, at the same droplet load, the flame radius $\widetilde{R}_f$ is shown to increase with the vaporization Damköhler number, Da_V, since Da_V is proportional to the fuel vaporization rate.

The flame temperature, $\widetilde{T}_f$, is shown in Fig. 3 as a function of the mass flow rate, $\widetilde{m}$, for $Le = 1.0$ and $\Delta = 0.2$. It is seen that $\widetilde{T}_f$ always decreases as $\widetilde{m}$ increases. This can be explained by the comparison between radiative loss and chemical heat release, as conducted by Wang and Chao [21] for purely gaseous spherical diffusion flame. The radiative loss rate is proportional to the volume of the heat loss region, which is roughly equal to the area of the flame sheet ($4\pi\widetilde{R}_f^2$) multiplying the thickness of the radiation region. Since the thickness of the radiation region is nearly independent of the $\widetilde{m}$ and $\widetilde{R}_f$ is roughly proportional to $\widetilde{m}$ (see Fig. 3), the radiative loss rate is proportional to the square of mass flow rate. The chemical heat release is proportion to the mass flow rate itself. Therefore, the ratio between radiative loss and chemical heat release increases with the mass flow rate, which makes $\widetilde{T}_f$ decrease with $\widetilde{m}$. It is also observed in Fig. 3 that the flame temperature $\widetilde{T}_f$ decreases with the radiation intensity Λ_R^*. Furthermore, it is noted that the zeroth order behavior of the flame (e.g., $\widetilde{R}_f$ and $\widetilde{T}_f$) is controlled by the competition between the radiative loss (which is proportional to $\widetilde{R}_f^2$) and latent heat absorption for droplet evaporation (which is proportional to Da_V). At relatively low radiation intensity of $\Lambda_R^* = 10^{-7}$ (see Fig. 3) the effect of latent heat absorption is dominant and hence the spray flame temperature is less than that of the purely gaseous flame at a given mass flow rate. However, at relatively high radiation intensity of $\Lambda_R^* = 10^{-5}$, the effect of radiative loss is dominant and the radiation intensity of the spray flame is weaker than that of the purely gaseous flame because the former has smaller flame radius (see Fig. 2) and and thereby lower radiative loss. Consequently, the flame temperature of spray combustion is larger than that of the purely gaseous combustion for $\Lambda_R^* = 5 \times 10^{-5}$ as shown in Fig. 3.

Unlike previous studies (e.g., [2–4,7,9,21,42]) only considering unity Lewis numbers, in this work the Lewis numbers of fuel and oxidizer can be nonunity (however we assume that the fuel and oxidizer have the same Lewis number). In Fig. 4 we plot the flame radius and flame temperature at different Lewis numbers for $\Delta = 0.2, Da_V = 10^{-4}$ and $\Lambda_R^* = 10^{-6}$. The flame radius and flame temperature are shown to strongly depend on the Lewis numbers. It is observed that the flame radius increases with the Lewis number. Consequently, the radiative loss becomes stronger at larger Lewis number. This causes lower flame temperature at larger Lewis number as shown in Fig. 4. According to Figs. 2–4, we can conclude that droplet evaporation and Lewis number influence both flame radius and flame temperature while the radiative loss only affects the flame temperature.

To stabilize the diffusion flame away from the burner, an $O(1)$ amount of fuel vapor cannot exist in the oxidizer side. This is because if both fuel and oxidizer exist in the oxidizer region, the diffusion flame will ignite the premixture to establish a premixed flame. The presence of the premixed flame then depletes the oxidizer, resulting in transient movement of the diffusion towards the oxidizer side. Therefore, it is necessary to assess the amount of fuel vapor in the oxidizer region for the spray diffusion flame considering finite-rate evaporation of droplet fuel. We plot the mass fraction of fuel vapor for fuels with different evaporation rates in Fig. 5. For the low volatility fuel, Fig. 5(a) shows that droplets can pass the flame front and then continue to evaporate into fuel vapor. However, the fuel vapor from droplet evaporation in the oxidizer region quickly diffuses into the reaction layer. Therefore, Y_F is an $O(\epsilon)$ quantity in the oxidizer region. For the high volatility fuel, Fig. 5(b) indicates that in the oxidized region, the mass fractions of droplet and fuel vapor are both nearly zero. Therefore, for the spray diffusion flame with finite-rate vaporization droplets, the fuel vapor concentration is an $O(\epsilon)$ quantity in the oxidizer region and spray diffusion flame can be stabilized.

Given the sensitivity of flame extinction to liquid transport properties and assumptions made in this study, we mainly focus on small initial droplet load (i.e., $\Delta = 0.2$) in the following analysis of flame extinction.

4.2. Kinetic extinction limit

At finite reaction rate (i.e., finite reduced reaction Damköhler number Λ_K^*), flame extinction occurs when the reaction rate becomes too slow. The extinction limits of spherical spray diffusion

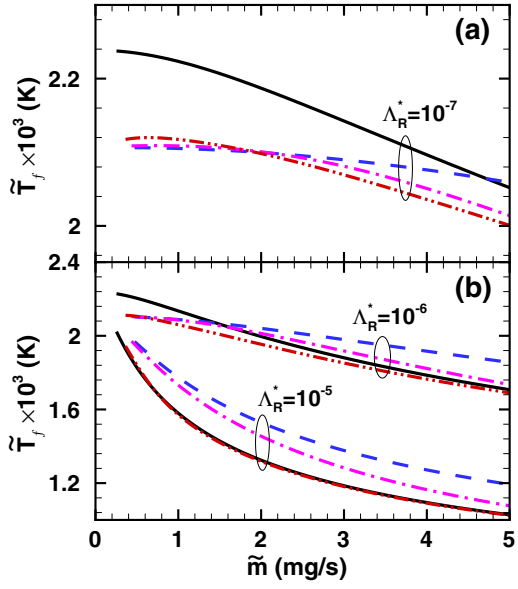

Fig. 3. Change of flame temperature, $\widetilde{T}_f$, with mass flow rate, $\widetilde{m}$, at $Le = 1.0$ and $\Delta = 0.2$. Solid lines: $\Delta = 0.0$; dashed lines: $Da_V = 10^{-6}$; dash-dotted lines: $Da_V = 10^{-4}$; dash-dot-dotted lines: $Da_V = 10^{-2}$.

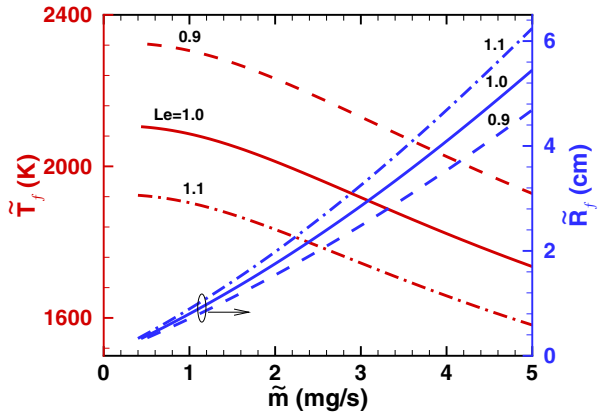

Fig. 4. Change of flame radius, $\widetilde{T}_f$, and flame radius, $\widetilde{R}_f$, with mass flow rate, $\widetilde{m}$, at $\Delta = 0.2, Da_V = 10^{-4}$, and $\Lambda_R^* = 10^{-6}$.

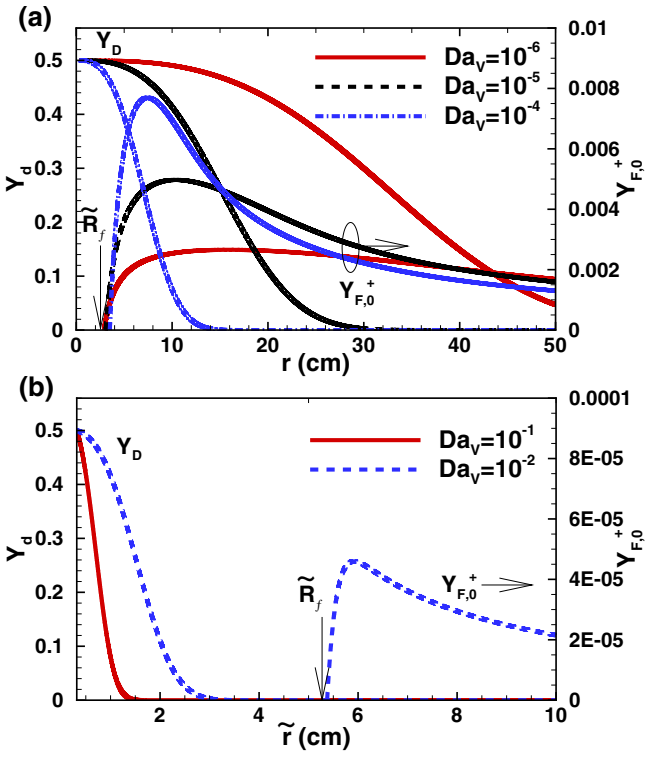

Fig. 5. Distributions of the mass fraction of droplet fuel, Y_d, and the zero order mass fraction of fuel vapor, $Y^+_{F,0}$, at $\tilde{m} = 2$ mg/s and $\Delta = 0.5$ for (a) low volatility and (b) high volatility fuels.

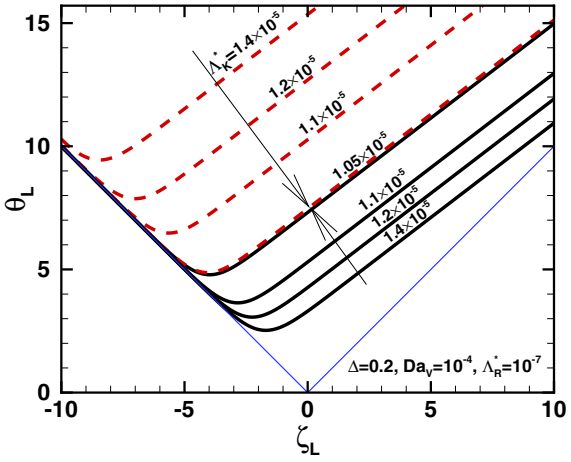

Fig. 6. The internal structure of the reaction zone of the spherical spray diffusion flame at $\tilde{m} = 2$ mg/s, $\Delta = 0.2$, $Da_V = 10^{-4}$ and $\Lambda^*_R = 10^{-7}$. Solid lines: stable solutions; dashed lines: unstable solutions.

flame can be investigated by solving the flame structure function in Eq. (77). The internal structure of the reaction zone in the spherical spray diffusion flame is shown in Fig. 6 for $\tilde{m} = 2$ mg/s, $\Delta = 0.2, Da_V = 10^{-4}$ and $\Lambda^*_R = 10^{-7}$. It is seen that two solutions exists for a given value of Λ^*_K when it is higher than a critical value. This critical reduced reaction Damköhler number is identified as the extinction state, $\Lambda^*_{K,E}$. Below the critical value $\Lambda^*_{K,E}$, no solution exists and flame extinction occurs. Unlike the purely gaseous flames [2], the slope of the curve at $\zeta_L \to +\infty$ is not equal to unity according to Eq. (80). This is due to the heat absorption by droplet evaporation, which can significantly affects $\Lambda^*_{K,E}$.

The fuel leakage can be used to investigate the extinction phenomena of diffusion flame (e.g., [21]). Fig. 7 shows the variation of fuel leakage $Y^*_{F,L}$ with the reduced reaction Damköhler number Λ^*_K at $\tilde{m}$=2 mg/s. The lower and middle branches of the well-known S-shaped ignition/extinction curve are shown in Fig. 7. The results of the purely gaseous flame (i.e., $\Delta = 0$) are included for comparison. In Fig. 7, the extinction state, $\Lambda^*_{K,E}$, is reached at the turning point which is denoted by open circle. There are two branches of solutions for fuel leakage when $\Lambda^*_K > \Lambda^*_{K,E}$. Only the lower branch is physically realistic since the fuel leakage $Y^*_{F,L}$ should increase as the extinction limit is approached. As expected, the value of $\Lambda^*_{K,E}$ is shown to increase greatly with radiation intensity. Moreover, the influence of droplet evaporation on the extinction state $\Lambda^*_{K,E}$ is shown to depend on the radiation intensity. This is due to the fact that the flame structure is affected by droplet evaporation in two ways: (1) the latent heat absorbed for droplet vaporization reduces the flame temperature; and (2) the decrease in the flame radius (see Fig. 2) results in the reduction of radiative loss (which is proportional to the square of flame radius) and residence time. Here the residence time refers to the time allowed for the fuel to pass through the reaction region and is inversely proportional to the flow speed [21]. For adiabatic (i.e., $\Lambda^*_R = 0.0$) or low radiation intensity (e.g., $\Lambda^*_R = 10^{-7}$) case, heat loss due to the latent heat absorbed for evaporation and decrease in the residence time due to relatively small flame radius induced by droplet evaporation are dominant. Consequently, the presence of droplets results in the larger value of $\Lambda^*_{K,E}$ than that of purely gaseous flame. Especially for lower vaporization Damköhler number (e.g., $Da_V = 10^{-6}$), the residence time is shorter and the flame is easier to be extinguished. However, at relatively high radiation intensity (e.g., $\Lambda^*_R = 10^{-6}$), the reduction of radiative loss due to the presence of droplet evaporation becomes dominant. As a result, the spray flame with the lower Da_V (e.g., $Da_V = 10^{-6}$) has lower $\Lambda^*_{K,E}$ than that of the purely gaseous flame. This indicates that the flame with higher radiation intensity and lower vaporization Damköhler number is relatively more difficult to be extinguished. It is noted that above extinction limit that is induced by lower reaction rate exists even without radiative loss. Therefore, it is the kinetic extinction limit. Since for a given mass flow rate, the flame radius is kept unchanged and radiative loss only weakens the flame and promotes kinetic extinction, the radiative extinction limit does not exist at higher values of Λ^*_K. This was also demonstrated by Wang and Chao [21] for purely gaseous spherical diffusion flame.

To demonstrate the effects of Lewis number, in Fig. 8 we plot the fuel leakage $Y^*_{F,L}$ as a function of the reaction Damköhler number Λ^*_K for the adiabatic ($\Lambda^*_R = 0.0$) and radiative ($\Lambda^*_R = 10^{-6}$) spherical spray diffusion flames at different Lewis numbers. It is observed that the kinetic extinction becomes more difficulty to happen at smaller Lewis number and thus $\Lambda^*_{K,E}$ increases with the Lewis number. This is due to that the flame temperature increases when the Lewis number decreases, as shown in Fig. 4. The results in Fig. 8 indicate that even a small deviation of the Lewis number from unity can result in the significant change in the kinetic extinction limit. Similar change was also observed in previous studies for purely gaseous diffusion flames [5,13].

4.3. Radiative extinction limit

In this subsection we investigate the radiative extinction limit. As mentioned before, the radiative extinction limit does not exist for a given mass flow rate. Therefore, in order to get the radiative extinction limits, the mass flow rate should change as an independent variable so that long residence time occurs. The leakage of

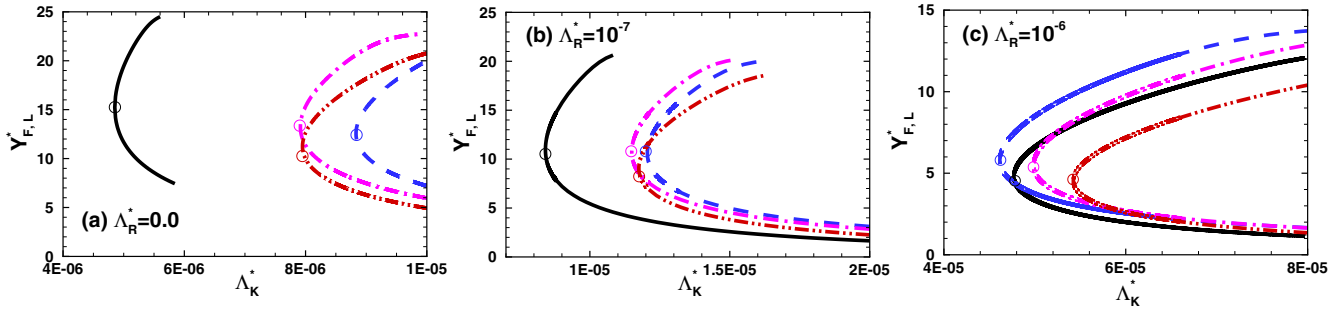

Fig. 7. Effect of radiative loss and droplet evaporation on fuel leakage, $Y_{F,L}^*$, at $\widetilde{m} = 2$ mg/s, $Le = 1.0$ and $\Delta = 0.2$. Solid lines: $\Delta = 0.0$, dashed lines: $Da_V = 10^{-6}$; dash-dotted lines: $Da_V = 10^{-4}$; dash-dot-dotted lines: $Da_V = 10^{-2}$. The open circles denote the kinetic extinction limits.

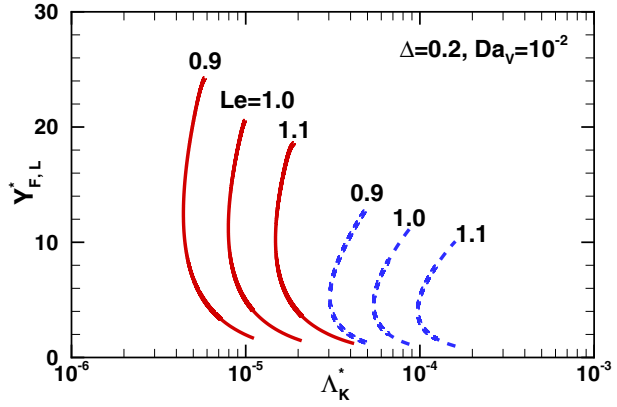

Fig. 8. Effect of radiative loss and Lewis number on fuel leakage, $Y_{F,L}^*$, at $\widetilde{m} = 2$ mg/s. Solid lines: $\Lambda_R^* = 0.0$; dashed lines: $\Lambda_R^* = 10^{-6}$.

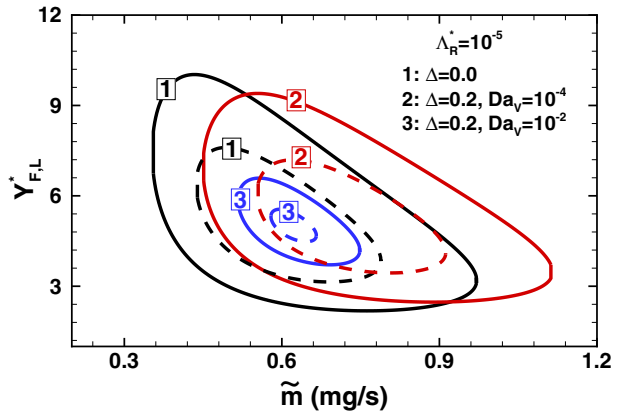

Fig. 9. Fuel leakage, $Y_{F,L}^*$, as a function of mass flow rate, $\widetilde{m}$, at $Le = 1.0$ and $\Lambda_R^* = 10^{-5}$. Solid lines: $\Lambda_K^* = 5.0 \times 10^{-4}$; dashed lines: $\Lambda_K^* = 4.5 \times 10^{-4}$.

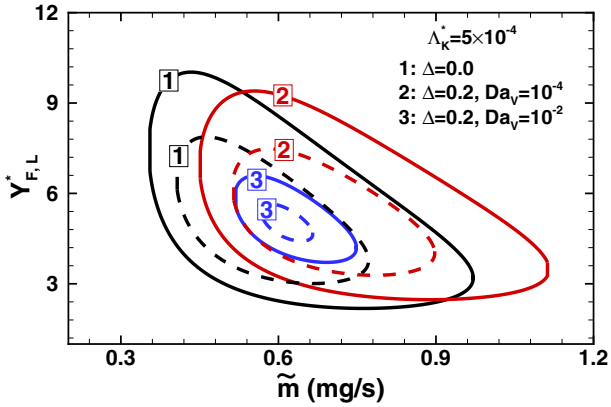

Fig. 10. Fuel leakage, $Y_{F,L}^*$, as a function of mass flow rate, $\widetilde{m}$, at $Le = 1.0$ and $\Lambda_K^* = 5 \times 10^{-4}$. Solid lines: $\Lambda_R^* = 10^{-5}$; dashed lines: $\Lambda_R^* = 1.1 \times 10^{-5}$.

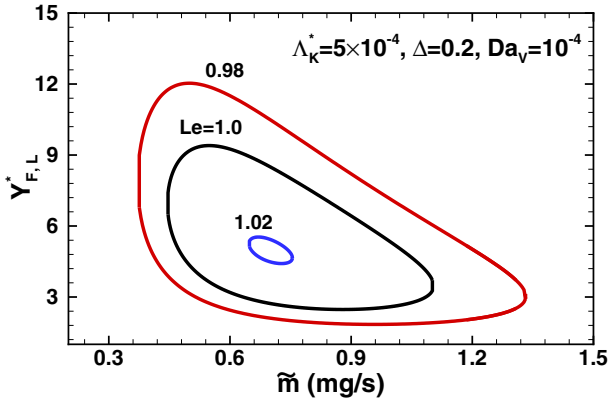

Fig. 11. Fuel leakage, $Y_{F,L}^*$, as a function of mass flow rate, $\widetilde{m}$, at different Lewis numbers.

fuel, $Y_{F,L}^*$, is plotted versus the mass flow rate, $\widetilde{m}$, in Figs. 9–11 for different cases. It is seen that for each case, spherical spray diffusion flame exists only when the mass flow rate is between a minimum value and a maximum value. The minimum and maximum mass flow rates correspond to the kinetic and radiative extinction limits, respectively. Within these two limits, two branches of solutions are observed and only the lower branch is physically realistic. Along the lower branch of solution, the fuel leakage, $Y_{F,L}^*$, first decreases and then increases with $\widetilde{m}$. This was explained by Wang and Chao [21] for purely gaseous spherical diffusion flame: it is mainly due to the fact that the chemical heat release rate is linearly proportional to the mass flow rate $\widetilde{m}$ while the radiative loss rate scale with $\widetilde{m}^2$. At low mass flow rate, the flame radius and radiative loss are both small and thereby it is mainly controlled by the residence time. (Since $\widetilde{m} \sim \widetilde{R}_f^2(\widetilde{\rho}\widetilde{u})_f$ and flame radius $\widetilde{R}_f$, we have $\widetilde{u} \sim \widetilde{m}^{-1}$. The residence time is inversely proportional to flow speed and thereby it is proportional to $\widetilde{m}$). When the mass flow rate increases, the residence time becomes longer and thereby the reaction becomes stronger such that the fuel leakage is reduced. At the large mass flow rate, the flame is mainly controlled by radiative loss. Since the ratio between radiative heat loss and chemical heat release rate is linearly proportional to the mass flow

rate, the fuel leakage increase with the mass flow rate when then radiative extinction limit is approached.

In Fig. 9 we show the results at different reduced reaction Damköhler numbers Λ_K^* for gaseous and spray diffusion flames. The flammable range between the kinetic and radiative extinction limits is shown to become narrower as Λ_K^* decreases from 5.0×10^{-4} to 4.5×10^{-4}. This is because the reaction rate is proportional to Λ_K^* and extinction occurs more easily at lower reaction rate. Moreover, the extinction limits and flammable range are shown to be greatly affected by droplet evaporation. It is seen that the minimum mass flow rate, corresponding to the kinetic extinction limit, always increases due to the presence of droplet vaporization and it further increases with increasing Da_V. This is due to short residence time and heat loss induced by droplet vaporization. However, the maximum mass flow rate, corresponding to the radiation extinction limit, changes with Da_V in non-monotonic way: it first increases at $Da_V = 10^{-4}$ and then decreases at $Da_V = 10^{-2}$. This is caused by the competition between the reduction in radiative loss due to small flame radius and the decrease in flame temperature due to the latent heat absorbed for droplet vaporization. At higher vaporization Damköhler number, $Da_V = 10^{-2}$, the latter effect is dominates and thereby flame extinction occurs more easily. Similar to Fig. 9, Fig. 10 shows the results at different radiation intensities. It is seen that the flammable region is reduced by increasing the radiative loss intensity (Λ_R^* from 10^{-5} to 1.1×10^{-5}), which implies that there exists a maximum Λ_R^* above which no flame exists.

The effects of Lewis number on both extinction limits are demonstrated in Fig. 11. The flammable region in terms of mass flow rate $\widetilde{m}$ is shown to be very sensitive to the Lewis number. Specifically, the region is greatly enlarged/narrowed when the Lewis number is slightly smaller/larger than unity. This is due to the fact that the change of Lewis number significantly affects flame temperature and flame radius. Therefore, for large hydrocarbon fuels with high Lewis number, the mass flow rate needs to be properly chosen in order to maintain the spherical diffusion flame. Furthermore, Fig. 4 and Fig. 11 indicate that the flame is affected by the Lewis number through both the zeroth order and the first order behavior of the flame, which is consistent with results reported in [5].

5. Conclusions

Spherical burner-stabilized diffusion flames with radiative loss and finite-rate droplet evaporation are analyzed using multiscale asymptotic method. Analytical correlations for flame radius, flame temperature and extinction limits are derived and used to examine the effects of finite-rate droplet evaporation on flame radius, flame temperature, and kinetic and radiative extinction limits. The main conclusions are:

When the mass flow rate is fixed and the reaction intensity varies, there only exists the conventional kinetic extinction limit characterized by a critical reaction Damköhler number. The extinction Damköhler number increases with the radiation intensity. It is strongly affected by droplet vaporization in two ways: (1) the latent heat absorbed for droplet vaporization reduces the flame temperature; and (2) the decrease in the flame radius results in the decrease in radiative loss and residence time. At lower radiation intensity, spray flames are much easier to be extinguished due to the decrease in the residence time induced by droplet evaporation. However, at higher radiation intensity, the spray flame with the lower vaporization Damköhler number is relatively more difficult to be extinguished. Furthermore, small deviation of the Lewis number from unity can result in significantly change of the kinetic extinction limit.

When the reaction intensity is fixed and the mass flow rate changes, there exists two extinction limits: a kinetic extinction limit at the low-flow rate and a radiative extinction limit at the high-flow rate. Therefore, steady spray flames only exist in the certain range of mass flow rate. This range becomes narrower when the reaction/radiation intensity decreases/increases. The flammable range is significantly affected by droplet evaporation and is also very sensitive to Lewis number. Therefore, a proper mass flow rate is needed in order to maintain steady diffusion flames for high-volatility fuel and/or fuels with large Lewis numbers.

It is noted that the present analysis is based on the assumptions of one-step irreversible reaction with large activation energy and quasi-monodisperse model for the spray. Moreover, the droplets are viewed from a dilute spray region which means the small volume fraction of liquid phase. It is neglected that the detailed heat transfer between droplet and gas phase. Therefore, the above conclusions only hold for fast chemistry with low heat release and dilute droplets with low droplet load. Detailed numerical simulations need to be performed so that the above assumptions can be relaxed and quantitative information can be provided for the extinction of spherical burner-stabilized diffusion spray flames. Nevertheless, qualitative results on extinction can still be provided in the present analysis considering one-step chemistry and quasi-monodisperse spray.

Acknowledgements

This work was supported by National Natural Science Foundation of China (Nos. 51322602 and 51136005).

References

[1] C.K. Law, Combustion Physics, Cambridge University Press, 2006.
[2] A. Liñán, The asymptotic structure of counterflow diffusion flames for large activation energies, Acta Astronaut. 1 (7) (1974) 1007–1039.
[3] C.K. Law, Asymptotic theory for ignition and extinction in droplet burning, Combust. Flame 24 (1975) 89–98.
[4] L. Krishnamurthy, F.A. Williams, K. Seshadri, Asymptotic theory of diffusion-flame extinction in the stagnation-point boundary layer, Combust. Flame 26 (1976) 363–377.
[5] S.H. Chung, C.K. Law, Structure and extinction of convective diffusion flames with general lewis numbers, Combust. Flame 52 (1983) 59–79.
[6] C.K. Law, S.H. Chung, Steady state diffusion flame structure with lewis number variations, Combust. Sci. Technol. 29 (3–6) (1982) 129–145.
[7] S.H. Sohrab, A. Liñan, F.A. Williams, Asymptotic theory of diffusion-flame extinction with radiant loss from the flame zone, Combust. Sci. Technol. 27 (3–4) (1982) 143–154.
[8] J.S. T'ien, Diffusion flame extinction at small stretch rates: the mechanism of radiative loss, Combust. Flame 65 (1) (1986) 31–34.
[9] B.H. Chao, C.K. Law, J.S. T'ien, Twenty-third symposium (international) on combustion structure and extinction of diffusion flames with flame radiation, Symp. (Int.) Combust. 23 (1) (1991) 523–531.
[10] K. Maruta, M. Yoshida, H. Guo, Y. Ju, T. Niioka, Extinction of low-stretched diffusion flame in microgravity, Combust. Flame 112 (1–2) (1998) 181–187.
[11] Y. Ju, H. Guo, K. Maruta, T. Niioka, Flame bifurcations and flammable regions of radiative counterflow premixed flames with general lewis numbers, Combust. Flame 113 (4) (1998) 603–614.
[12] F. Liu, G. Smallwood, Ö. Gülder, Y. Ju, Asymptotic analysis of radiative extinction in counterflow diffusion flames of nonunity lewis numbers, Combust. Flame 121 (1–2) (2000) 275–287.
[13] J.S. Kim, F.A. Williams, Extinction of diffusion flames with nonunity lewis numbers, J. Eng. Math. 31 (2–3) (1997) 101–118.
[14] H. Wang, W. Chen, C.K. Law, Extinction of counterflow diffusion flames with radiative heat loss and nonunity lewis numbers, Combust. Flame 148 (3) (2007) 100–116.
[15] K. Mills, M. Matalon, Burner-generated spherical diffusion flames, Combust. Sci. Technol. 129 (1–6) (1997) 295–319.
[16] K. Mills, M. Matalon, Extinction of spherical diffusion flames in the presence of radiant loss, Symp. (Int.) Combust. 27 (2) (1998) 2535–2541.
[17] S. Yoo, E. Christiansen, C. Law, Oscillatory extinction of spherical diffusion flames: micro-buoyancy experiment and computation, Proc. Combust. Inst. 29 (1) (2002) 29–36.
[18] S.D. Tse, D. Zhu, C.-J. Sung, Y. Ju, C.K. Law, Microgravity burner-generated spherical diffusion flames: experiment and computation, Combust. Flame 125 (4) (2001) 1265–1278.

[19] S. Tang, M.K. Chernovsky, H.G. Im, A. Atreya, A computational study of spherical diffusion flames in microgravity with gas radiation part i: model development and validation, Combust. Flame 157 (1) (2010) 118–126.
[20] S. Tang, M.K. Chernovsky, H.G. Im, A. Atreya, A computational study of spherical diffusion flames in microgravity with gas radiation part i: model development and validation, Combust. Flame 157 (1) (2010) 118–126.
[21] Q. Wang, B.H. Chao, Kinetic and radiative extinctions of spherical burner-stabilized diffusion flames, Combust. Flame 158 (8) (2011) 1532–1541.
[22] S.C. Li, P.A. Libby, F.A. Williams, Twenty-fourth symposium on combustion experimental and theoretical studies of counterflow spray diffusion flames, Symp. (Int.) Combust. 24 (1) (1992) 1503–1512.
[23] J.B. Greenberg, I. Shpilberg, Lewis number and vaporization effects in spray diffusion flames, Atomization Sprays 3 (1993) 437–462.
[24] I.S. Wichman, M. Yang, Double-spray counterflow diffusion flame model, Combust. Theor. Model. 2 (4) (1998) 373–398.
[25] J.B. Greenberg, N. Sarig, Coupled evaporation and transport effects in counterflow spray diffusion flames, Combust. Sci. Technol. 92 (1–3) (1993) 1–33.
[26] A. Dvorjetski, J.B. Greenberg, Influence of non-unity lewis numbers and droplet loading on the extinction of counter-flow spray diffusion flames, Proc. Combust. Inst. 28 (1) (2000) 1047–1054.
[27] A. Dvorjetski, J.B. Greenberg, Analysis of extinction of counterflow polydisperse spray diffusion flames by a polydisperse water spray, Proc. Combust. Inst. 29 (1) (2002) 385–392.
[28] J.B. Greenberg, A. Dvorjetski, Opposed flow polydisperse spray diffusion flames: Steady state and extinction analysis, Combust. Theor. Model. 7 (1) (2003) 145–162.
[29] A. Dvorjetski, J.B. Greenberg, Theoretical analysis of polydisperse water spray extinction of opposed flow diffusion flames, Fire Saf. J. 39 (4) (2004) 309–326.
[30] J.B. Greenberg, D. Katoshevski, Analysis of a spray diffusion flame and its extinction in a shear layer, Combust. Theor. Model. 13 (2) (2009) 215–234.
[31] J.B. Greenberg, D. Katoshevski, A new solution for a polydisperse spray diffusion flame and its extinction in a shear layer, Proc. Combust. Inst. 34 (1) (2013) 1617–1624.
[32] V.S. Santoro, D.C. Kyritsis, A. Gomez, An experimental study of vortex-flame interaction in counterflow spray diffusion flames, Proc. Combust. Inst. 28 (1) (2000) 1023–1030.
[33] V.S. Santoro, D.C. Kyritsis, A. Liñán, A. Gomez, Vortex-induced extinction behavior in methanol gaseous flames: a comparison with quasi-steady extinction, Proc. Combust. Inst. 28 (2) (2000) 2109–2116.
[34] M. Mikami, S. Miyamoto, N. Kojima, Counterflow diffusion flame with polydisperse sprays, Proc. Combust. Inst. 29 (1) (2002) 593–599.
[35] M.N. Sasongko, M. Mikami, A. Dvorjetski, Extinction condition of counterflow diffusion flame with polydisperse water sprays, Proc. Combust. Inst. 33 (2) (2011) 2555–2562.
[36] R.J. Kee, K. Yamashita, H. Zhu, A.M. Dean, The effects of liquid-fuel thermophysical properties, carrier-gas composition, and pressure, on strained opposed-flow non-premixed flames, Combust. Flame 158 (6) (2011) 1129–1139.
[37] C. Wang, A.M. Dean, H. Zhu, R.J. Kee, The effects of multicomponent fuel droplet evaporation on the kinetics of strained opposed-flow diffusion flames, Combust. Flame 160 (2) (2013) 265–275.
[38] H. Zhu, Y. Zhang, M. Xu, R.J. Kee, Droplet vaporization characteristics of multicomponent mixtures of methanol and gasoline surrogate in opposed stagnation flows, Proc. Combust. Inst. 34 (1) (2013) 1545–1552.
[39] C. Wang, A.M. Dean, H. Zhu, R.J. Kee, Model-predicted effects of fuel droplet diameter and addition in strained, opposed-flow, non-premixed, multicomponent, hydrocarbon flames, Combust. Flame 161 (8) (2014) 1998–2007.
[40] P.B. Sunderland, R.L. Axelbaum, D.L. Urban, B.H. Chao, S. Liu, Effects of structure and hydrodynamics on the sooting behavior of spherical microgravity diffusion flames, Combust. Flame 132 (1–2) (2003) 25–33.
[41] K.J. Santa, B.H. Chao, P.B. Sunderland, D.L. Urban, D.P. Stocker, R.L. Axelbaum, Radiative extinction of gaseous spherical diffusion flames in microgravity, Combust. Flame 151 (4) (2007) 665–675.
[42] S. Liu, B.H. Chao, R.L. Axelbaum, A theoretical study on soot inception in spherical burner-stabilized diffusion flames, Combust. Flame 140 (1–2) (2005) 1–23.
[43] J.B. Greenberg, A. McIntosh, J. Brindley, Linear stability analysis of laminar premixed spray flames, Proc. R. Soc. London, A: Math. Phys. Eng. Sci. 457 (2005) (2001) 1–31.
[44] C. Nicoli, P. Haldenwang, S. Suard, Analysis of pulsating spray flames propagating in lean two-phase mixtures with unity lewis number, Combust. Flame 143 (3) (2005) 299–312.
[45] J.B. Greenberg, Finite-rate evaporation and droplet drag effects in spherical flame front propagation through a liquid fuel mist, Combust. Flame 148 (4) (2007) 187–197.
[46] W. Han, Z. Chen, Effects of finite-rate droplet evaporation on the ignition and propagation of premixed spherical spray flame, Combust. Flame 162 (5) (2015) 2128–2139.
[47] A.L. Sánchez, J. Urzay, A. Liñán, The role of separation of scales in the description of spray combustion, Proc. Combust. Inst. 35 (2) (2015) 1549–1577.
[48] Y. Ju, G. Masuya, F. Liu, Y. Hattori, D. Riechelmann, Asymptotic analysis of radiation extinction of stretched premixed flames, Int. J. Heat Mass Transfer 43 (2) (2000) 231–239.
[49] Y. Tambour, Vaporization of polydisperse fuel sprays in a laminar boundary layer flow: a sectional approach, Combust. Flame 58 (2) (1984) 103–114.
[50] Y. Tambour, A lagrangian sectional approach for simulating droplet size distribution of vaporizing fuel sprays in a turbulent jet, Combust. Flame 60 (1) (1985) 15–28.
[51] J.B. Greenberg, I. Silverman, Y. Tambour, A new heterogeneous burning velocity formula for the propagation of a laminar flame front through a polydisperse spray of droplets, Combust. Flame 104 (3) (1996) 358–368.
[52] C. Nicoli, P. Haldenwang, S. Suard, Effects of substituting fuel spray for fuel gas on flame stability in lean premixtures, Combust. Flame 149 (3) (2007) 295–313.
[53] A.H. Lefebvre, Atomization and Sprays, Taylor and Francis, 1989.